Phosphorus fuels *Cladophora* growth and self-reinforcing adhesion via extracellular polysaccharides on hard substrata

Yifan Du[a,c,#] Siguang Yuan[b,#] Jinyi Qin[c] Siming Jiao[d] Yufan Ai[a,g] Yingjie Li[a,g] Nan Li[b] Xiaonan Chen[b,e,f] Xiaoming Cai[d] Xinzong Xiao[b,e,f,*] Jilong Wang[a] Min Yang[a,g] Ming Su[a,g,*]

[#] These authors contributed equally to this work.

[a] Key Laboratory of Environmental Aquatic Chemistry, State Key Laboratory of Regional Environment and Sustainability, Research Center for Eco-Environmental Sciences, Chinese Academy of Sciences, Beijing 100085, China.

[b] China South to North Water Diversion Middle Route Corporation Limited, Beijing 100038, China.

[c] School of Civil Engineering, Chang'an University, Xi'an 710064, China.

[d] Institute of Process Engineering, Chinese Academy of Sciences, Beijing 100190, China.

[e] Hubei Key Laboratory of Intelligent Monitoring, Early Warning and Protection for Watershed Aquatic Ecology, Wuhan 430010, China.

[f] Water Quality and Aquatic Ecosystem Observation and Research Station of South-to-North Water Diversion Middle Line Project, Beijing 100038, China.

[g] University of Chinese Academy of Sciences, Beijing 100049, China.

[*] Corresponding to: Xinzong Xiao (xiaoxinzong@csnwd.com.cn), Ming Su (mingsu@rcees.ac.cn)

Abstract

Although high flow velocity, low nutrients, and smooth concrete surfaces typically suppress benthic algae, the filamentous alga *Cladophora* formed extensive biofilms in a major water transfer canal under conditions typically unfavorable for benthic algal colonization, leading to filter clogging and challenging the operational stability of drinking-water treatment for 180 million people. Here, we quantified *Cladophora* biomass, extracellular polysaccharides (EPS), and nanoscale adhesion through field surveys along the 1197 km canal, laboratory P-enrichment experiments. P enrichment increased acid-extracted polysaccharides (APS) yield per biomass by 21.6 %, and native EPS–sediment adhesion reached 18.6 nN, with polysaccharide backbones contributing ~88%. Along the canal, APS and sediment P were positively associated ($p < 0.01$) and both peaked at 30–45 cm depth. These results support a positive feedback mechanism in which APS strengthens adhesion and promotes local retention of P-bearing particles, potentially increasing phosphorus accessibility at the algal–matrix interface and further stabilizing the biofilm. The same biofilm can detach and cause downstream clogging. This self-reinforcing mechanism explains the spatial persistence of *Cladophora* blooms and provides a predictive basis for managing risks in large-scale water conveyance systems.

Keywords: Long-distance water conveyance; Acid-extracted polysaccharides; Biofilm adhesion; Phosphorus sequestration; Filamentous green algae

1 Introduction

Continuous conveyance flow, low bulk nutrient concentrations, and smooth concrete surfaces (Cantonati and Lowe, 2014) typically constrain the initial attachment and retention of benthic algae. Yet under these apparently unfavorable conditions, extensive *Cladophora* biofilms developed on the walls of a 1197 km water-transfer canal in China and were periodically detached and transported downstream (Supplementary Fig. 1A-B). The entry of these detached aggregates into the water treatment plant leads to clogging of both intake screens and sand filters, directly threatening drinking water safety by shortening the backwash time by 48% (Supplementary Fig. 1C). For the world's largest water transfer project—serving 180 million people—this *Cladophora* bloom has implications for water supply security. The mechanisms by which the alga establishes and persists under high-flow, nutrient-poor, and hard-surface conditions remain unknown.

Cladophora is a widely distributed filamentous green alga capable of forming persistent mats across freshwater, brackish, and hypersaline environments. These mats can modify local physicochemical conditions, retain suspended material, and provide structurally complex habitats for associated organisms, supporting the recognition of *Cladophora* as an ecosystem engineer (Prazukin et al., 2025; Prazukin et al., 2020; Wang et al., 2024; Wu et al., 2024). Across these contrasting systems, phosphorus availability and underwater irradiance are major controls on seasonal biomass development (McCusker et al., 2023; Zulkifly et al., 2013).

While this environment-forming capacity is well documented in natural systems, its expression in engineered canals—where smooth concrete and continuous flow provide minimal physical anchoring—depends critically on successful establishment at the algal–substratum interface. Stabilization of this interface is therefore particularly important during the initial attached stage. Physiological studies have shown that *Cladophora* secretes extracellular polymeric substances (EPS), within which acidic polysaccharides (APS) enriched in rhamnose, galactose, and xylose constitute an important component of the cell wall-associated and extracellular matrix. Their negatively charged

functional groups interact with multivalent cations to form cross-linked polymeric networks, thereby strengthening matrix cohesion, interfacial adhesion, and resistance to hydraulic disturbance (Ciancia et al., 2020; Srisai et al., 2024; Surayot et al., 2016). Such interactions may be particularly relevant in concrete-lined canals, where smooth surfaces provide limited mechanical anchoring, while Ca-bearing mineral phases at the concrete–water interface can facilitate ion-mediated matrix stabilization and phosphorus retention (Akula et al., 2020; Penn et al., 2007). EPS enhances shear resistance under low-flow conditions (Bäcker et al., 2026; Ciancia et al., 2020). However, this knowledge comes predominantly from static or low-velocity laboratory setups, or from natural habitats where irregular substrates provide physical anchoring. Whether *Cladophora* can actively modify its local environment to reinforce attachment on smooth, high-shear concrete surfaces—and whether such modification creates a self-sustaining positive feedback—has never been tested.

We hypothesize that *Cladophora* colonization initiates a self-reinforcing loop in which initial attachment stimulates APS secretion. The resulting polysaccharide-rich matrix strengthens adhesion and promotes the retention of P-bearing particles, generating locally enriched sediment-associated and EPS-associated phosphorus pools at the attachment interface. Although these pools are not necessarily immediately bioavailable, subsequent desorption, dissolution, mineralization, or matrix–water exchange may increase phosphorus accessibility near the algal surface. Increased phosphorus supply may, in turn, promote further APS production and biomass accumulation, thereby stabilizing the biofilm under bulk oligotrophic and high-flow conditions. The same adhesive biofilm can, however, detach episodically during hydraulic fluctuations or seasonal senescence, and the released fragments cause downstream clogging. To test this hypothesis, we conducted a 1197 km field survey along a major canal, combined with laboratory phosphorus-enrichment and light-intensity experiments, and used atomic force microscopy (AFM) to measure nanoscale adhesion forces. Our integrated results support a positive-feedback mechanism of phosphorus-driven, self-reinforcing adhesion on hard substrata, providing a predictive basis for managing *Cladophora* risks in large-scale water conveyance systems.

2 Materials and methods

2.1 Study site and sampling collection

The study canal is a major inter-basin water transfer trunk with a trapezoidal cross-section, base width 15–30 m (varies along alignment), water depth 5–7 m, and concrete-lined walls. Design flow rate decreases from 320 $m^3 s^{-1}$ in the south to 165 $m^3 s^{-1}$ in the north. This smooth, hard substratum provides low initial roughness, so attached organisms depend on molecular adhesion. Between January 2020 and December 2024, about 150 sampling campaigns were conducted at ~30 stations spaced 30–50 km apart, with more frequent sampling during the algal growing season (July–September). Background environmental parameters (Supplementary Fig. 3, Supplementary Fig. 4, Supplementary Fig. 5) and basic water quality (Supplementary Table 1) were routinely recorded.

In 2022, an unprecedented *Cladophora* bloom occurred. A full-canal survey (July 5–8, including underwater robotic sampling) showed that the bloom was confined to the southernmost ~180 km reach. The survey also characterized the along-canal and vertical distribution of biomass and morphology (Supplementary Fig. 12).

To investigate the adhesion mechanism of *Cladophora* under contrasting hydraulic conditions, representative cross-sections were selected from the long-term monitoring network using a stratified sampling strategy. Site selection considered canal chainage, long-term observations of *Cladophora* growth, and engineering hydraulic characteristics, including flow velocity, hydraulic structures, and depositional conditions. Accordingly, the representative cross-sections were classified into an upstream reach (N01–N13), a hydraulic transition reach associated with the Yellow River crossing (N04–N05), and a downstream reach (N06–N13).Two additional sampling locations on the downstream branch canals were included in the depth-resolved survey, giving a total of 16 sampling locations (Supplementary Fig. 2). At each section, three points were sampled on the left wall, right wall, and channel center. Stratified sampling was performed at six depths (15, 30, 45, 60, 75, 90 cm below the surface) on the sloping walls. At each depth, sediment total phosphorus (TP), *Cladophora* EPS, and algal biomass

were measured.

Cladophora biomass was harvested by scraping a 30 cm × 30 cm quadrat on the concrete wall (0–30 cm below surface). Attached algae were removed with a stiff brush, surface water drained, and wet weight recorded. Surface water (0–50 cm), mid-depth water (60–90 cm), near-bottom water, and surface sediment (0–5 cm, collected with a Petersen grab) were also sampled. Part of the *Cladophora* material was reserved for morphological observation; the remainder was stored at 4 °C for EPS extraction and chlorophyll-*a* (Chl-*a*) analysis.

2.2 In-situ water quality and laboratory analyses

Water temperature, pH, dissolved oxygen (DO), conductivity, and turbidity were measured in the field with a YSI EXO2 multiparameter sonde. *Cladophora* biomass was recorded as wet weight.

Chl-a was determined by hot-ethanol extraction and spectrophotometry. Fresh algae (~0.50 g wet weight) were blotted dry, transferred to a 15 mL centrifuge tube, and extracted with 10 mL of 90% (v/v) ethanol. The suspension was vortexed and incubated in the dark at 4 °C for 24 h with intermittent agitation. Samples were then heated at 80 °C for 15 min (protected from light), cooled to room temperature, and centrifuged at 8000 rpm for 10 min. The supernatant was adjusted to 10 mL with 90% ethanol. Absorbance was measured at 665, 649, and 750 nm against a 90% ethanol blank. Turbidity-corrected absorbances were $A_{665(\mathrm{corr})} = A_{665} - A_{750}$ and $A_{649(\mathrm{corr})} = A_{649} - A_{750}$. Chl-a concentration ($\mu$g mL^{-1}) was computed as:

$$\text{Chl-}a = 13.95 \times A_{665(\mathrm{corr})} - 6.88 \times A_{649(\mathrm{corr})} \tag{1}$$

Final Chl-a content is expressed as mg g^{-1} wet weight. All analyses were performed in triplicate (Supplementary Fig. 7).

Water samples collected during each campaign were analyzed for total nitrogen (TN), nitrate-nitrogen (NO_3^--N), ammonium-nitrogen (NH_4^+-N), total phosphorus (TP), and soluble reactive phosphorus

(SRP) following Chinese national standards: TN by alkaline potassium persulfate digestion-UV spectrophotometry (HJ 636-2012), TP by ammonium molybdate spectrophotometry (GB 11893-89), and chemical oxygen demand (COD) by potassium dichromate oxidation (HJ 828-2017). Sediment TP was determined by $HClO_4$–H_2SO_4 digestion followed by molybdate spectrophotometry; available phosphorus (Olsen-P) was extracted with 0.5 mol L^{-1} $NaHCO_3$ and analyzed by the molybdenum-blue method.

2.3 EPS extraction and compositional analysis

EPS was fractionated from *Cladophora* using a three-step sequential protocol. Soluble EPS (S-EPS) was obtained by suspending fresh algae in phosphate-buffered saline (PBS, pH 7.4) at a biomass-to-buffer ratio of approximately 40% (w/v), shaking at 100 rpm for 20 min, and centrifuging at 8000 rpm for 20 min; the supernatant was then filtered through a 0.22 μm membrane. Loosely bound EPS (LB-EPS) was extracted by resuspending the pellet in Tris-HCl buffer (pH 8.0) containing 0.3% (w/v) EDTA at the same biomass-to-buffer ratio, sonicating in an ice bath for 5 min, and centrifuging at 8000 rpm for 30 min; the supernatant was retained. Tightly bound EPS (TB-EPS) was obtained by suspending the remaining pellet in 50 mM NaCl buffer (pH 6.8) containing 0.1% (w/v) cellulase, incubating at 37 °C for 20 min and then at 40 °C for another 20 min, stopping the reaction by cooling on ice, and centrifuging at 12 000 rpm for 20 min. The three fractions were pooled, precipitated with 3 volumes of anhydrous ethanol at 5 °C for 12 h, collected by centrifugation at 5000 rpm, and lyophilized to obtain total EPS. Polysaccharide content was measured by the phenol-sulfuric acid method (glucose standard); protein content by the Coomassie Brilliant Blue G-250 method (bovine serum albumin standard). Total EPS yield is reported as the sum of polysaccharide and protein (mg g^{-1} wet weight) (Supplementary Fig. 8).

2.4 Light-intensity and phosphorus-supplementation experiments

Cladophora filaments were pre-cleaned and acclimated in the laboratory. Uniform segments (initial wet weight 0.50 g) were transferred to 500 mL flasks containing 300 mL of half-strength BG-11 olig-

otrophic medium (all nutrients except the manipulated variable at standard levels). Wet-to-dry ratio was determined as 22.0 ± 2.0% (dried at 60 °C to constant weight) for conversion to dry weight (Supplementary Fig. 9).

Light-intensity experiment: Five irradiance levels were used: 27, 54, 81, 108, and 135 μmol m^{-2} s^{-1} (12 h:12 h light-dark cycle, 23 °C), with three replicates each. The attenuation of photosynthetically active radiation with depth was modeled by the Lambert–Beer equation:

$$I(z) = I_0 \times \exp(-K_e \times z) \tag{2}$$

where I_0 is the incident subsurface irradiance (μmol m^{-2} s^{-1}), K_e is the diffuse attenuation coefficient (m^{-1}), and z is depth (m).

Phosphorus-addition experiment: To determine whether phosphorus enrichment specifically enhances APS allocation independently of algal biomass accumulation, *Cladophora* was cultivated under two phosphorus regimes: a phosphorus-supplemented treatment (0.0875 mM P as K_2HPO_4) and a phosphorus-limited control, while all other nutrients were maintained at half-strength BG-11 levels. A total of 15 culture flasks were allocated for biological replication and temporal sampling, with three independent replicates for each treatment at each sampling endpoint. Cultures were maintained at 23 °C under an irradiance of 80 μmol m^{-2} s^{-1} with a 12 h:12 h light-dark cycle for 52 days. Biomass was monitored every 48 h during medium renewal, and final biomass, EPS yield, APS content, and spore abundance were quantified at the end of the incubation. Accordingly, linear regression was used to compare the biomass–EPS and biomass–APS relationships, with differences in slopes indicating changes in biomass-specific polysaccharide production.

2.5 Atomic force microscopy force spectroscopy

Nanoscale adhesion between *Cladophora* EPS and canal sediment surfaces (or simulated cement substrates representing the concrete wall) was measured with a Bruker Dimension Icon atomic force mi-

croscope in force-spectroscopy mode. Total EPS was deposited as a film on freshly cleaved mica substrates (Supplementary Methods S1.1). RTESPA-150 probes were used for the general EPS–substrate adhesion measurements, with calibrated inverse optical lever sensitivity and spring constant values of 82 nm V^{-1} and 6.0 N m^{-1}, respectively. BL-AC40TS probes were used for the chemical perturbation experiments, with corresponding calibrated values of 20 nm V^{-1} and 0.10 N m^{-1}. Deflection sensitivity and spring constant were calibrated for each probe before measurement.Detailed procedures for EPS-film preparation are provided in Supplementary Methods S1-S3.

Measurements were conducted in PBS buffer (pH 7.4) at approach/retraction velocity of 1 μm s^{-1} and a trigger force of 5–10 nN. At least 10 random sites per sample were probed; at each site, 256 force-distance curves were acquired, with three independent biological replicates. Adhesion force (F) was calculated as $F = k \cdot \Delta d$, where k is the spring constant and Δd is the deflection change. All adhesion forces are reported as positive magnitudes. Raw force curves were processed with NanoScope Analysis software. Results are presented as mean ± standard deviation.

To identify the adhesive components within the EPS matrix, a stepwise perturbation experiment was conducted: (i) TFA hydrolysis, to disrupt the polysaccharide backbones; and (ii) subsequent β-glucuronidase digestion, to assess the additional involvement of residual glucuronic-acid-containing domains associated with acidic polysaccharides. Changes in adhesion force after each step were used to evaluate their relative involvement in EPS-mediated adhesion. Further methodological details are provided in Supplementary methonds S1.

2.6 Data analysis

Data were processed and analyzed using R version 4.3. One-way ANOVA followed by Tukey's HSD test was used for multiple comparisons. Linear regression was applied to evaluate the association between $\log_{10}(P_{\text{sed}})$ and $\log_{10}(\text{APS})$; model fit is reported as R^2 and p-value. Statistical significance was set at $p < 0.05$ unless otherwise stated (Supplementary Fig. 10, Supplementary Table 2).

3 Results and discussion

3.1 Spatiotemporal evolution of *Cladophora* growth in the conveyance canal

Cladophora biomass and colonization patterns varied markedly along the canal. The 2022 full-canal survey showed that the major bloom was confined to the southernmost approximately 180 km of the 1197 km canal. From the canal origin to 76 km, algal bands remained narrow and were concentrated in shallow, well-illuminated zones under relatively fast-flowing conditions (Reiss et al., 2023). Between 76 and 92 km, flow velocity decreased from 0.74 to 0.62 m s^{-1}, while sediment accumulation increased and algal bands widened markedly. This reach therefore represented the principal transition from restricted shallow colonization to extensive biomass accumulation (Supplementary Fig. 11; Supplementary Fig. 12). Further downstream, attached biomass declined progressively, confirming that sustained proliferation was spatially restricted rather than uniformly distributed along the canal (Supplementary Fig. 11, Supplementary Fig. 12).

The field survey also recorded a clear vertical organization of attached biomass. *Cladophora* was concentrated within illuminated regions of the canal slopes, while biomass declined beyond the effective light-penetration depth. Underwater light availability therefore defined the vertical growth range, whereas local flow and sediment retention controlled biomass accumulation within that range. This spatial pattern provided the field basis for the subsequent light-intensity experiment and the calculation of seasonally suitable colonization depths from water transparency. (Ben Salem et al., 2025; Xie et al., 2025; Yang et al., 2024).

The spatial development of attached biomass directly affected downstream treatment infrastructure. Samples collected from water-treatment-plant intake screens and manual harvests showed that detached *Cladophora* entered the treatment stream as entangled filament–particle composites rather than as isolated filaments (Supplementary Fig. 1B). Continuous filaments formed the structural framework of these aggregates, while EPS retained biofilm fragments and associated particles, producing

a mesh-like structure that accumulated on intake screens and within rapid sand filters (Shekhar et al., 2017). Long-term filter records showed that *Cladophora* sloughing progressively shortened the backwash interval, with an average reduction of approximately 48% across two independent filter units by the end of the observation period (Supplementary Fig. 1C), thereby increasing backwashing frequency, water consumption, energy demand, and operational pressure (Azizi et al., 2021; Zhang et al., 2016). These results establish the canal-scale distribution and downstream consequences of *Cladophora* proliferation and lead to the central mechanistic question addressed below: how phosphorus supply and underwater irradiance support persistent biomass accumulation and APS production under oligotrophic, high-flow conditions.

3.2 Co-regulation of *Cladophora* metabolism by phosphorus enrichment and light availability

P enrichment increased extracellular polysaccharide production relative to *Cladophora* biomass accumulation, whereas underwater irradiance determined the vertical range over which this response could support *Cladophora* colonization. During the 52-day cultivation, biomass followed similar trajectories in the two treatments during days 0–20 and diverged during days 20–30. The P-supplemented group reached a stationary phase after approximately day 30, maintaining a biomass level consistently higher than that of the P-limited group throughout the remainder of the experiment. Notably, EPS and APS yields in the P-supplemented treatment remained approximately twice those in the P-limited treatment over the entire 52-day period, indicating that phosphorus enrichment enhanced extracellular matrix production beyond its effect on biomass accumulation (Fig. 1A–C).

Regression analysis further distinguished extracellular matrix production from biomass accumulation. The EPS–biomass slope was 12.941 (R^2 = 0.517) under P supplementation and 10.364 (R^2 = 0.346) under P limitation, corresponding to a 24.8% increase (Fig. 1E). The APS–biomass slope increased from 213.89 in the P-limited treatment to 260.02 in the P-supplemented treatment, representing a 21.6 % increase (Fig. 1F). Thus, under P supplementation, each unit increase in biomass was

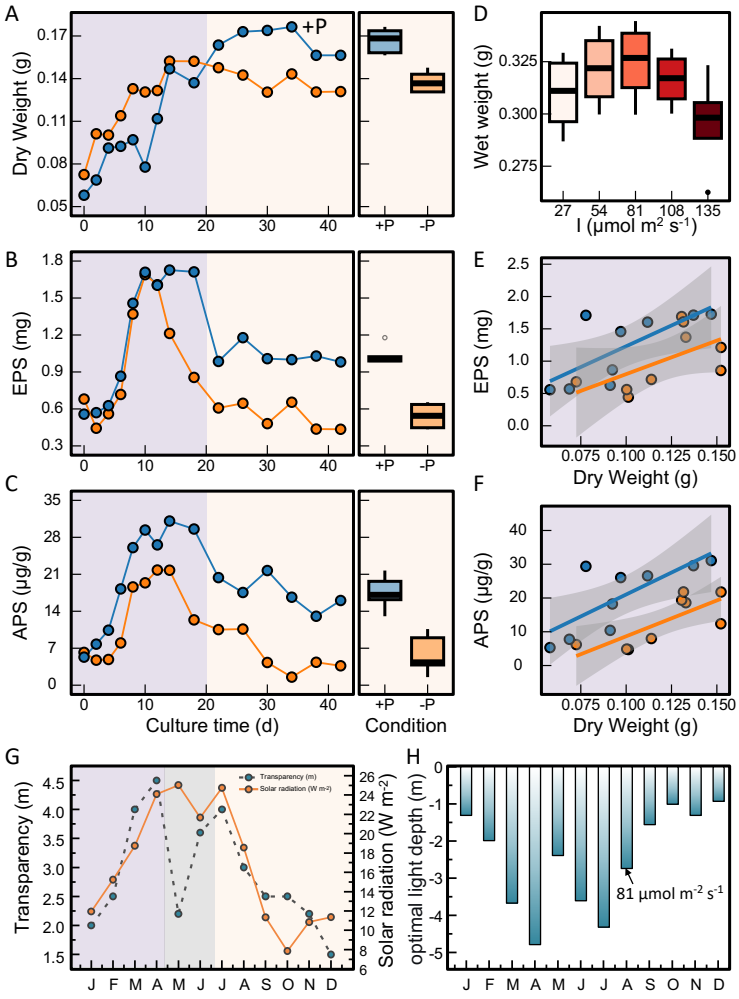

Fig. 1: Effects of phosphorus enrichment and irradiance on *Cladophora* growth, EPS secretion, and APS accumulation. (Upper row) Temporal dynamics of biomass (dry weight) under P-supplemented (+P, orange) and P-limited (−P, blue) conditions. (Middle left) Temporal dynamics of EPS yield. (Middle right) Temporal dynamics of APS yield. (D) Boxplot of wet-weight distribution across five irradiance levels (27, 54, 81, 108, 135 µmol m^{-2} s^{-1}). (E) Allometric scatter plot and linear regression of biomass versus EPS (orange = +P, blue = −P). (F) Allometric scatter plot and linear regression of biomass versus APS. (G) Seasonal migration of optimal growth depth (bar chart) and (H) seasonal variation in the diffuse attenuation coefficient (K_e).

associated with greater EPS and APS production. This response is consistent with the capacity of *Cladophora* to acquire and retain phosphorus beyond its immediate growth demand (Stevenson and Stoermer, 1982). Because acidic-polysaccharide-rich domains contribute to the structural integrity and interfacial adhesion of the EPS matrix, the increase in APS production links elevated P supply to the development of an adhesion-supporting extracellular matrix (Li et al., 2022).

Irradiance determined the light conditions under which biomass development was maximized.

Across the five tested irradiance levels, biomass reached its maximum at 81 μmol m^{-2} s^{-1}, with a mean wet weight of 0.314 g (Fig. 1D). This irradiance was therefore defined as the optimal growth irradiance under the tested oligotrophic conditions. The decrease in biomass above this level was consistent with the nutrient-dependent light response reported for green macroalgae (Oikawa et al., 2022; Park et al., 2025).

Seasonal simulations using twelve months of monitoring data translated this experimentally determined optimum into a vertical colonization depth (Fig. 1G, H). The predicted optimal depth reached 4.79 m in April and 4.32 m in October, when underwater light attenuation was lowest, and shifted upward to 0.93 m in December as attenuation increased. The resulting seasonal range of 0.93–4.79 m was comparable to the reported 0.5–5.0 m colonization range of *Cladophora* in large freshwater systems (Dodds et al., 1999; Zribi et al., 2023) (Supplementary Table 3, Supplementary Fig. 13). These results establish water transparency as a quantitative predictor of the canal-slope depth at which irradiance is most favorable for *Cladophora* growth.

The seasonal displacement of the predicted growth depth reflects compensation for changes in underwater irradiance. Irradiance near 81 μmol m^{-2} s^{-1} provides light conditions associated with high photochemical performance and net primary productivity in attached algae (Chua et al., 2024; Schubert et al., 2024). During biomass accumulation, canopy self-shading further reduces the irradiance received by underlying filaments (Kirk, 1975), whereas senescence and decomposition increase organic matter and turbidity, strengthen light attenuation, and contract the illuminated growth zone (Yunev et al., 2007). These biomass-mediated changes modify the realized vertical distribution around the transparency-derived optimum and support the use of seasonal light attenuation for identifying canal-slope zones vulnerable to *Cladophora* colonization.

3.3 Spatial coupling and vertical stratification of sediment phosphorus and APS

Sediment phosphorus (P_{sed}), EPS, and APS exhibited spatially related but non-identical longitudinal and depth-dependent distributions along the canal (Fig. 2A–C). Across all sites, the 30 cm layer had the highest mean concentrations of EPS (21.12 μg g^{-1}), APS (0.42 μg g^{-1}), and P_{sed} (40.63 mg kg^{-1}), and also showed the greatest among-site variability. This layer therefore represented the principal depth at which sediment-P accumulation and extracellular-matrix retention overlapped. Sediment-derived EPS and APS are expressed per unit dry sediment mass, whereas the cultivation data in Section 3.2 were normalized to wet algal biomass.

The longitudinal maxima of sediment P and APS were spatially offset. At 30 cm, P_{sed} reached 102.54, 99.87, and 91.32 mg kg^{-1} at N01, N02, and N03, respectively, defining the principal upstream P-enrichment zone. APS did not peak at these P-rich sites; instead, its maximum concentration of 1.19 μg g^{-1} occurred at N05, where P_{sed} was 66.78 mg kg^{-1}. At the same site, EPS increased from 10.12 μg g^{-1} at 15 cm to 27.37 μg g^{-1} at 45 cm, locating the major extracellular-polymer retention zone within the 30–45 cm interval.

The offset between the upstream P_{sed} maxima and the APS maximum at N05 defined a transition from P-rich sediment accumulation to localized polysaccharide retention. Across the canal, the strongest overlap among P_{sed}, EPS, and APS occurred at 30 cm, whereas their relative distributions varied across deeper layers and downstream reaches. The following subsections therefore examine this spatial pattern along two complementary dimensions: depth-resolved stratification and longitudinal variation in relation to canal hydraulics.

3.3.1 Depth profiles and vertical stratification

Vertical profiles from 16 sites showed distinct depth distributions of sediment phosphorus (P_{sed}) and APS (Fig. 3A, B). Mean P_{sed} reached a maximum of 39.8 mg kg^{-1} at 30 cm and decreased to 26.3 mg kg^{-1} at 90 cm. The 30 cm layer also exhibited the widest among-site distribution, indicating that spatial

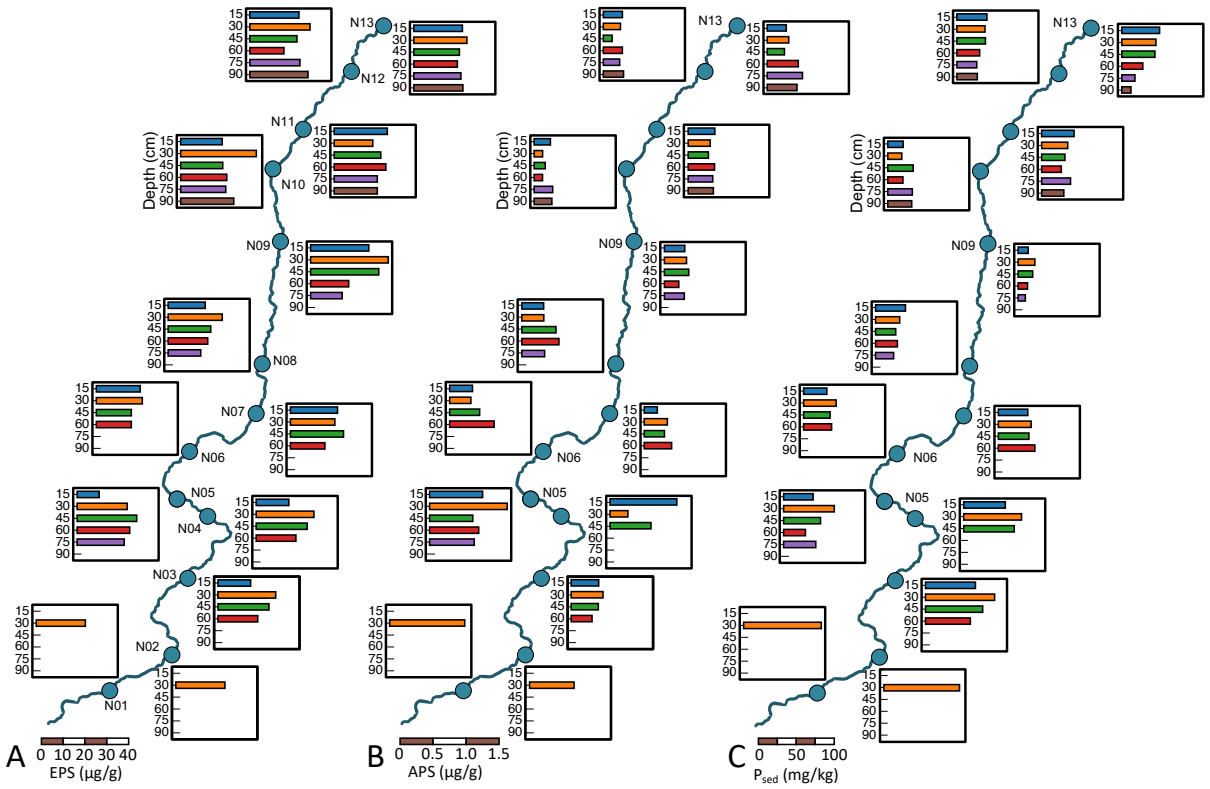

Fig. 2: Spatial–vertical distributions of EPS, APS, and sediment phosphorus along the canal. The blue curve denotes the canal route; filled circles mark sampling cross-sections (N01–N13). Horizontal bar charts adjacent to each cross-section display depth-stratified distributions at 15, 30, 45, 60, 75, and 90 cm, with colour gradation from shallow (light) to deep (dark). (A) EPS content (μg g^{-1}); (B) APS content (μg g^{-1}); (C) sediment total phosphorus P_{sed} (mg kg^{-1}).

differences in sediment-P accumulation were most strongly expressed at this depth.

APS exhibited a deeper maximum than P_{sed}, reaching 0.35–0.45 μg g^{-1} within the 45–60 cm interval. The vertical offset between the two maxima defined a stratified retention structure: P-bearing particles were concentrated primarily near 30 cm, whereas APS was retained more strongly within the deeper 45–60 cm layer. Reduced exposure to near-surface disturbance at these depths favors the preservation of cohesive polysaccharide matrices, while adsorption and physical entrapment within the matrix can prolong the residence of associated particles (Boult et al., 2006; Clarke, 2002; Gerbersdorf et al., 2009). Site-specific profiles showed that the position of this interface varied along the canal. At N05, APS reached 1.19 μg g^{-1} at 30 cm and EPS increased from 10.12 μg g^{-1} at 15 cm to 27.37 μg g^{-1} at 45 cm, while the non-monotonic P_{sed} profile indicated sediment redistribution through resuspension and

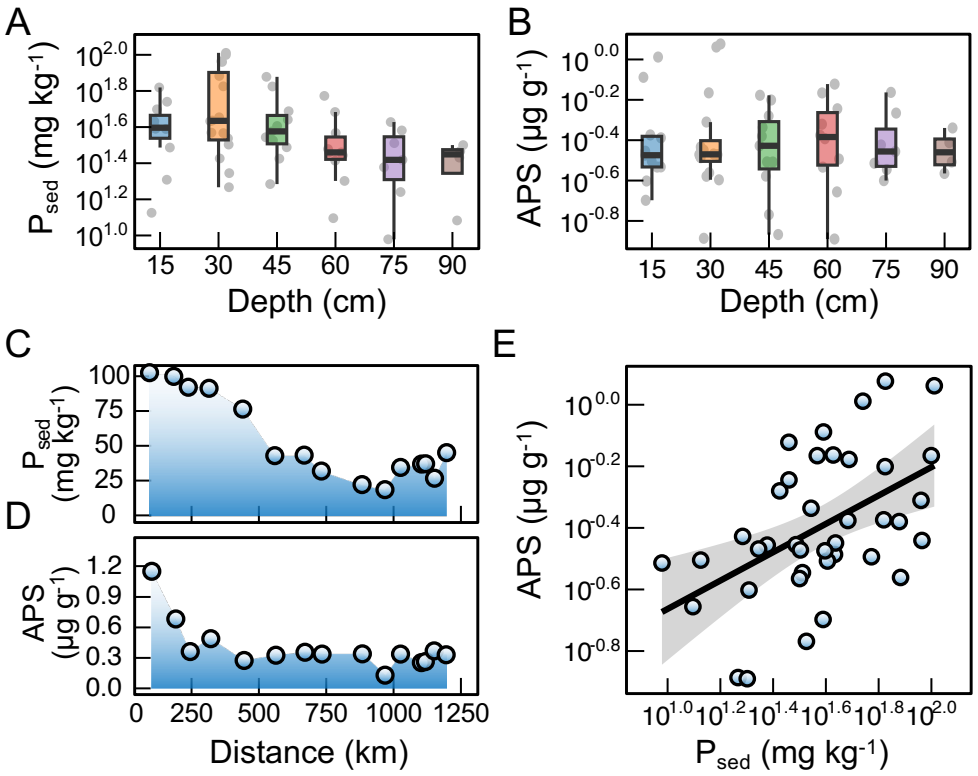

Fig. 3: Depth-resolved and spatial distributions of sediment phosphorus and APS along the 1197 km trunk canal. (A) Boxplot of P_{sed} across sampling depths (15–90 cm) on a logarithmic y-axis (10^x), with grey scatter points showing raw data dispersion. (B) Boxplot of APS content across sampling depths, illustrating vertical stratification of polysaccharide components. (C) Longitudinal trend of P_{sed} (0–1250 km) with blue gradient indicating concentration intensity. (D) Longitudinal trend of APS with canal length; inset shows localized APS elevation associated with micro-gastropod proliferation. (E) Log-transformed regression between P_{sed} and APS. The black line indicates the fitted regression and grey shading denotes the 95% confidence interval.

redeposition (Guo et al., 2022; Xu et al., 2020). At N13, APS shifted from 0.17–0.25 μg g^{-1} at 15–30 cm to 0.46–0.55 μg g^{-1} at 60–90 cm, confirming that the depth of polysaccharide preservation was not uniform among reaches.

The vertical profiles therefore define a stratified attachment interface in which sediment-P accumulation was concentrated primarily near 30 cm, whereas APS preservation extended into the 45–60 cm layer. Their overlapping distributions across 30–60 cm identify this interval as the principal zone where particle deposition and extracellular-matrix retention converged (Battin et al., 2016). The longitudinal variation in the position and magnitude of this interface is examined below in relation to canal hydraulics.

3.3.2 Longitudinal patterns and hydrodynamic modulation

Along the canal, sediment P and APS also varied with hydraulics (Fig. 3C,D). At 30 cm, P_{sed} reached 102.54, 99.87, and 91.32 mg kg^{-1} at N01, N02, and N03, respectively, defining the principal upstream P-enrichment zone. APS did not reach its maximum at these P-rich sites. Instead, the highest APS concentration occurred at N05 (484 km), where APS reached 1.19 μg g^{-1} and P_{sed} was 66.78 mg kg^{-1}. The offset between the P_{sed} and APS maxima marked a transition from upstream P-rich sediment accumulation to localized polysaccharide retention.

The APS maximum at N05 coincided with a local proliferation of small gastropods with shell lengths below 1 cm. Gastropod grazing, nutrient recycling, surface disturbance, and mucus production can modify periphytic biomass and extracellular-matrix composition (Arakelova, 2010; Armenio et al., 2015; Liegertová and Malý, 2023). These processes provide an ecological context for the local APS maximum, although the relative contributions of algal APS and gastropod-derived polysaccharides were not quantified. More broadly, the N05 transition is consistent with the combined regulation of periphytic biomass by nutrient supply, light availability, and near-bed disturbance (Bravo et al., 2019; Che et al., 2022; Flynn et al., 2018; Hui et al., 2021).

In the terminal reach (1026–1119 km), lower conveyance energy allowed suspended particles and nutrients to settle, creating a stable substrate for attachment. Together with light conditions near the optimal irradiance (81 μmol m^{-2} s^{-1}), this favored persistence of filamentous green algae. Across all sites, P_{sed} and APS showed a significant positive relationship in log-transformed space: $\log_{10}(APS) = 0.4606 \log_{10}(P_{sed}) - 1.124$, $R^2 = 0.2508$, $p < 0.01$ (Fig. 3E). P-enriched sediments are thus generally associated with more APS (Li et al., 2015). However, the moderate R^2 and wide scatter indicate that sediment P alone does not control APS accumulation (Paul et al., 2012). Instead, APS integrates effects of P availability, hydrodynamic retention, and algal biomass persistence (Flemming and Wingender, 2010). The moderate correlation (compared to the strong P-dependence in laboratory cultures, +21.6 % APS per biomass) shows that hydraulics and physical disturbance substantially modulate this biochemical response in situ. APS-rich matrices may retain P-associated particles through

electrostatic interactions, complexation, and physical entrapment, supporting localized phosphorus buffering at the water–alga–sediment interface rather than uniform sequestration across the canal (Lu et al., 2016).This field-scale spatial relationship provides the basis for the subsequent analysis of the mechanical contribution of the retained polysaccharide matrix to *Cladophora* attachment.

3.4 Macroscale biofilm accumulation and engineering implications

Submerged attachment plates provided a standardized measure of biofilm accumulation and retention along the canal, complementing observations of the pre-existing natural algal bands. Visible *Cladophora* attachment occurred within the upstream 0–400 km reach, whereas the 400–559 km reach was characterized by erosion scars and sparse algal cover (Fig. 4A). Recolonization occurred downstream of 731 km, and the highest plate-associated biomass was recorded in the terminal 1119–1197 km reach. This longitudinal sequence delineated an intermediate erosion-dominated reach and downstream retention zones, where reduced conveyance energy coincided with increased particle settling and filament accumulation (Cembella et al., 1984; Serrano-Ruiz et al., 2011).

To see how local hydrodynamics affect matrix preservation, we compared P_{sed}, APS, and EPS on the front and side faces of the plates (Fig. 4B–D). P_{sed} differed little between side and front (31 vs. 29 mg kg^{-1}), indicating comparable P backgrounds. But APS and EPS were clearly higher on the side face: 0.63 μg g^{-1} and 35 μg g^{-1}, respectively. Thus local matrix accumulation depends not just on P availability but on surface exposure and retention capacity. The front face, hit by flow, turbulence, and sediment abrasion, has short particle residence and loses loosely attached algae and EPS. In contrast, lateral flow creates sheltered side-face microzones; repeated abrasion also forms pits, grooves, and roughened protrusions that anchor residual or dormant *Cladophora* filaments. Their retention favors APS preservation and EPS accumulation, which in turn strengthens algal–substrate adhesion and traps P-associated particles via electrostatic attraction and physical filtration (Chen et al., 2020; Kawaguchi and Decho, 2002; Murugavel et al., 2008). Hence side-face enrichment of APS/EPS shows that local hydrodynamic sheltering and roughened attachment sites, not P alone, control the persistence of polysaccharide-rich layers. Sheltered side microzones not only allow initial colonization but

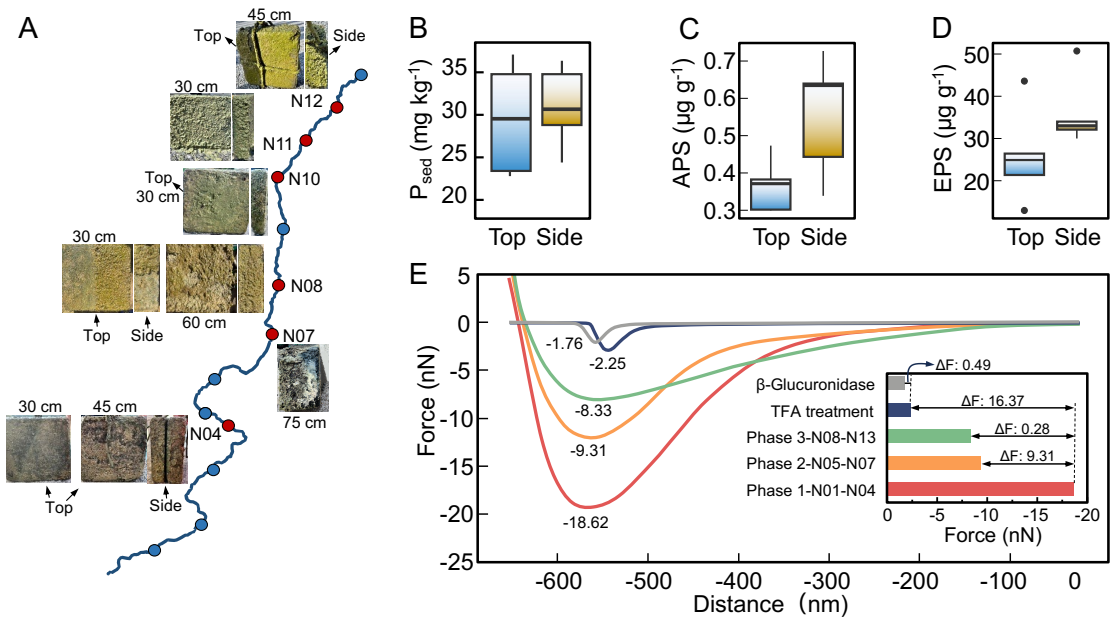

Fig. 4: Macroscopic morphology of attached biofilms and AFM-measured nanoscale adhesion at representative sampling sites. (A) Spatial distribution of sampling sites (blue curve = canal route, 0–1440 km; red circles = sites with photographic documentation) and macroscopic photographs of biofilm morphology at different depths (15–90 cm). (B–D) Comparison of P_{sed} (B), APS (C), and EPS (D) contents between the top (high-shear) and side (low-shear) surfaces of attachment plates. (E) Representative AFM force–distance retraction curves of native EPS and EPS films treated with TFA hydrolysis or β-glucuronidase digestion.

also promote self-reinforcing adhesion: once APS accumulates, it increases surface roughness and electrostatic binding, further enhancing particle retention and EPS production independent of bulk P concentration.

Atomic force microscopy (AFM) force spectroscopy distinguished the structural and chemical contributions of *Cladophora* EPS to nanoscale adhesion during the substrate-attached stage. Among the tested groups, native EPS exhibited the highest mean adhesion force of 18.62 nN (Fig. 4E). Sequential deconstruction was applied. Trifluoroacetic acid (TFA) hydrolysis, which breaks long-chain polysaccharides, reduced the force from 18.62 to 2.25 nN (a loss of 16.37 nN). This large drop shows that the extended polysaccharide network dominates interfacial energy dissipation. Subsequent β-glucuronidase treatment further lowered residual adhesion to 1.76 nN (an additional 0.49 nN). This smaller but measurable decrease suggests that glucuronic-acid-containing domains contribute to residual specific adhesion after backbone disruption, but are not the sole adhesive determinant (Alfinaikh et al., 2025; Wang et al., 2026). The AFM results thus indicate a hierarchical adhesion

mechanism: the polysaccharide backbone provides the main mechanical framework for interfacial toughness, while acidic groups aid localized substrate recognition and residual binding.

Though 18.6 nN is a nanoscale force, micrometre-scale contact spacing suggests EPS-mediated contacts could reach ~10^{12} m^{-2} on biofilm surfaces (Neu and Lawrence, 2006; Staudt et al., 2004). This scaling supports the relevance of nanoscale adhesion to attachment-layer persistence, though direct microscopic validation is needed. From a biogeochemical view, this nanomechanical reinforcement may stabilize the organic–inorganic interface at the sediment surface and promote retention of P-bearing fine particles, providing a microscale explanation for the field-observed link between APS enrichment and P_{sed} accumulation (Li et al., 2025).

3.5 Mechanistic synthesis and management implications

Integrating laboratory, field, and AFM evidence, we propose a mechanistic sequence linking phosphorus supply, extracellular-matrix production, attachment-layer stabilization, and downstream transport.The APS-rich matrix strengthens adhesion and promotes retention of P-bearing particles, enriching an EPS-associated P pool at the algal–substratum interface. Once retained, organic P within this pool may be hydrolyzed by extracellular phosphatases secreted by *Cladophora* and its associated epiphytes (Song et al., 2017), thereby increasing local inorganic P availability under phosphate-deficient conditions. This enzymatic pathway thus complements physical P retention (Fig. 5). Initial attachment on smooth concrete relies on EPS. Where phosphorus is available, *Cladophora* increases APS secretion by 21.6 % per unit biomass under P enrichment. The APS-rich matrix strengthens algal–substratum adhesion to 18.6 nN, with polysaccharide backbones contributing about 88% of this force. Stronger adhesion reduces shear-induced detachment and promotes the retention of P-bearing particles, enriching an EPS-associated extractable P pool near the algal–substratum interface and potentially increasing local P accessibility. The resulting P retention–APS production feedback may reinforce biofilm accumulation even under bulk oligotrophic and high-flow conditions.Because the present water-column, sediment-associated, and EPS-associated P measurements characterize spatial P enrichment and association rather than the chemical speciation or direct assimilation of the retained

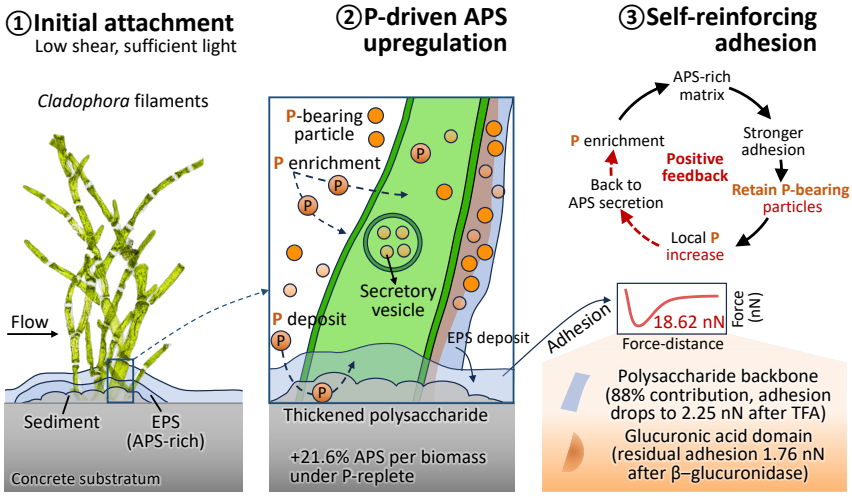

Fig. 5: Conceptual diagram of the positive feedback loop in *Cladophora* colonization on concrete. (1) Initial attachment under low shear and light. (2) P-driven APS secretion strengthens adhesion (18.6 nN). (3) Trapped particles raise local P, further stimulating APS production. Detachment under high shear or senescence causes downstream clogging.

phosphorus, the inferred increase in local P accessibility should be interpreted as a mechanistic inference. Further integration of P-fractionation, release-kinetics, and algal-uptake measurements would help determine which retained P pools contribute most directly to sustaining this feedback.

Once established, the polysaccharide matrix prolonged the residence of fine particles and associated P at the algal–substratum interface through electrostatic association, complexation, and physical entrapment. Organic P retained within or adjacent to the matrix may subsequently be hydrolyzed by extracellular phosphatases, thereby increasing local inorganic-P availability under phosphate-deficient conditions (Song et al., 2017). The combined effects of physical retention and enzymatic mobilization may support further biomass and matrix production. However, the measured water-column, sediment-associated, and EPS-associated P pools characterize spatial enrichment and association rather than the chemical speciation, release, or direct algal assimilation of the retained P. Further P-fractionation, release-kinetics, and algal-uptake measurements are therefore required to identify which retained P pools contribute directly to sustaining this feedback.

This retention-based feedback promotes persistent colonization under moderate-flow conditions but also increases downstream risk when the attachment layer is destabilized. Flow fluctuations, main-

tenance flushing, and seasonal senescence can detach mature biofilm fragments ranging from individual filaments to mesh-like filament–particle composites. Once mobilized, these aggregates are transported downstream and accumulate on intake screens and within rapid sand filters, increasing clogging and backwash demand. The mechanism therefore links two canal-scale observations: persistent *Cladophora* accumulation in reaches where hydraulic retention and P availability support matrix development, and elevated treatment-plant maintenance following episodic detachment and downstream transport of adhesive biomass.

Based on the proposed P retention–APS production feedback, management should focus on interrupting local P accumulation and biofilm maturation before the adhesion cycle becomes self-reinforcing. In the historical bloom core within the southernmost approximately 180 km, particularly the depositional reach at 76–92 km, underwater surveys should be conducted in April, followed by targeted sediment removal and slope cleaning in May–June before the principal July–September growth period. Inspection should cover the predicted seasonal colonization range of 0.93–4.79 m, with priority given to the 30–60 cm attachment interface where sediment P and APS were concentrated. A follow-up survey in October could identify residual mats associated with deeper light penetration.

Hydraulic regulation should avoid prolonged low-flow deposition and uncoordinated high-shear flushing. Where water-delivery requirements permit, sustained velocities at or below approximately 0.5 m s^{-1} should be avoided in recurrent depositional reaches, while a provisional operating range of 0.60–0.70 m s^{-1} may limit fine-particle settling without the energy demand of whole-canal high-flow operation. Sectional flushing of established mats should be coordinated with temporary interception at downstream control structures and forebays, followed by intensified mechanical removal at canal screens and treatment-plant intakes. This integrated strategy combines depth-guided monitoring, localized desilting and slope cleaning, hydraulic regulation, and canal–plant interception to reduce both biofilm development and downstream clogging.

4 Conclusion

Across the 1197 km water-transfer canal, recurrent *Cladophora* colonization was concentrated within the first ~180 km, where underwater irradiance, local hydraulics, and P availability jointly favored the establishment of substrate-attached biomass. Laboratory experiments further showed that P regulated not only biomass development but also extracellular-matrix production, as indicated by a 21.6 % increase in the APS–biomass regression slope under P supplementation. This enhanced capacity for matrix formation was functionally linked to attachment: disruption of the extended polysaccharide network reduced mean EPS adhesion from 18.62 to 2.25 nN, demonstrating its central role in stabilizing the attached layer. Combined with the field association between sediment P and APS, these findings support a self-reinforcing P retention–matrix production mechanism in which P promotes biomass and adhesive-matrix formation, while the retained matrix stabilizes colonization and concentrates P-bearing material at the algal–concrete interface, potentially supporting further matrix development. This mechanism provides a coherent explanation for the recurrent occupation of favorable canal-wall habitats under oligotrophic and continuously flowing conditions. Accordingly, management should focus on interrupting matrix establishment and interfacial P retention in hotspot reaches before mature biomass detaches, complemented by downstream interception to protect treatment facilities.

CRediT authorship contribution statement

[Author One]: Conceptualization, Methodology, Writing – original draft. [Author Two]: Investigation, Formal analysis. [Corresponding Author]: Writing – review & editing, Supervision, Funding acquisition.

Declaration of competing interest

The authors declare that they have no known competing financial interests or personal relationships that could have appeared to influence the work reported in this paper.

Data availability

Data will be made available on request.

Acknowledgements

This work was financially supported by Funder name (Grant No. …).

References

Akula, P., Hariharan, N., Little, D.N., Lesueur, D., Herrier, G., 2020. Evaluating the long-term durability of lime treatment in hydraulic structures: Case study on the friant-kern canal. Transportation Research Record: Journal of the Transportation Research Board 2674, 431–443. https://doi.org/10.1177/0361198120919404

Alfinaikh, R.S., Alamry, K.A., Hussein, M.A., 2025. Sustainable and biocompatible hybrid materials-based sulfated polysaccharides for biomedical applications: A review. RSC Advances 15, 4708–4767. https://doi.org/10.1039/d4ra07277d

Arakelova, E.S., 2010. Periphyton grazing and phosphorus excretion by mollusks. Russian Journal of Ecology 41, 327–332. https://doi.org/10.1134/s1067413610040089

Armenio, P.M., Mayer, C.M., Heckathorn, S.A., Bridgeman, T.B., Panek, S.E., 2015. Resource contributions from dreissenid mussels to the benthic algae *Lyngbya wollei* (cyanobacteria) and *Cladophora glomerata* (chlorophyta). Hydrobiologia 763, 35–51. https://doi.org/10.1007/s10750-015-2357-3

Azizi, S., Hashemi, A., Pajoum Shariati, F., Tayebati, H., Keramati, A., Bonakdarpour, B., A. Shirazi, M.M., 2021. Effect of different light-dark cycles on the membrane fouling, eps and smp production in a novel reciprocal membrane photobioreactor (rmpbr) by c. Vulgaris species. Journal of Water Process Engineering 43, 102256. https://doi.org/10.1016/j.jwpe.2021.102256

Bäcker, M., Doekes, H.M., Garza, D.R., Meijer, J., Vliet, S. van, Allen, R.J., Hogeweg, P., Dutilh, B.E., Dijk, B. van, 2026. Spatial structure: Shaping the ecology and evolution of microbial communities. FEMS Microbiology Reviews 50. https://doi.org/10.1093/femsre/fuaf067

Battin, T.J., Besemer, K., Bengtsson, M.M., Romani, A.M., Packmann, A.I., 2016. The ecology and biogeochemistry of stream biofilms. Nature Reviews Microbiology 14, 251–263. https://doi.org/10.1038/nrmicro.2016.15

Ben Salem, D., Yahiaoui, K., Bernardo, M., Gatica, J.M., Ouakouak, A., Touahra, F., Saad Eltaweil, A., Tran, H.N., 2025. Insights into cadmium adsorption characteristics and mechanisms by new granular alginate hydrogels reinforced with biochar: Important role of cation exchange. Journal of Environmental Management 383, 125407. https://doi.org/10.1016/j.jenvman.2025.125407

Boult, S., Hand, V.L., Vaughan, D.J., 2006. Microbial controls on metal mobility under the low nutrient fluxes found throughout the subsurface. Science of The Total Environment 372, 299–305. https://doi.org/10.1016/j.scitotenv.2006.08.043

Bravo, H.R., Bootsma, H., Khazaei, B., 2019. Fate of phosphorus from a point source in the lake michigan nearshore zone. Journal of Great Lakes Research 45, 1182–1196. https://doi.org/10.1016/j.jglr.2019.09.007

Cantonati, M., Lowe, R.L., 2014. Lake benthic algae: Toward an understanding of their ecology. Fresh-

water Science 33, 475–486. https://doi.org/10.1086/676140

Cembella, A.D., Antia, N.J., Harrison, P.J., Rhee, G.-Y., 1984. The utilization of inorganic and organic phosphorous compounds as nutrients by eukaryotic microalgae: A multidisciplinary perspective: Part 2. CRC Critical Reviews in Microbiology 11, 13–81. https://doi.org/10.3109/10408418409105902

Che, W., Liu, J., Hao, S., Ren, J., Song, Z., Bu, F., 2022. Application of colloid-sand coating treated by a hydrophilic polysaccharide biopolymer material for topsoil stability control. Geoderma 424, 115994. https://doi.org/10.1016/j.geoderma.2022.115994

Chen, D., Jia, J., Liao, X., Zhou, L., Hu, Z.-T., Pan, B., 2020. Phosphate removal by polystyrene anion exchanger (psax)-supporting Fe-loaded nanocomposites: Effects of psax functional groups and ferric (hydr)oxide crystallinity. Chemical Engineering Journal 387, 124193. https://doi.org/10.1016/j.cej.2020.124193

Chua, S.T., Smith, A., Murthy, S., Murace, M., Yang, H., Schertel, L., Kühl, M., Cicuta, P., Smith, A.G., Wangpraseurt, D., Vignolini, S., 2024. Light management by algal aggregates in living photosynthetic hydrogels. Proceedings of the National Academy of Sciences 121. https://doi.org/10.1073/pnas.2316206121

Ciancia, M., Fernández, P.V., Leliaert, F., 2020. Diversity of sulfated polysaccharides from cell walls of coenocytic green algae and their structural relationships in view of green algal evolution. Frontiers in Plant Science 11. https://doi.org/10.3389/fpls.2020.554585

Clarke, S.J., 2002. Vegetation growth in rivers: Influences upon sediment and nutrient dynamics. Progress in Physical Geography: Earth and Environment 26, 159–172. https://doi.org/10.1191/0309133302pp324ra

Dodds, W.K., Biggs, B.J.F., Lowe, R.L., 1999. Photosynthesis-irradiance patterns in benthic microalgae: Variations as a function of assemblage thickness and community structure. Journal of Phycology 35, 42–53. https://doi.org/10.1046/j.1529-8817.1999.3510042.x

Flemming, H.-C., Wingender, J., 2010. The biofilm matrix. Nature Reviews Microbiology 8, 623–633. https://doi.org/10.1038/nrmicro2415

Flynn, K.F., Chudyk, W., Watson, V., Chapra, S.C., Suplee, M.W., 2018. Influence of biomass and water velocity on light attenuation of *Cladophora glomerata* l. (Kuetzing) in rivers. Aquatic Botany 151, 62–70. https://doi.org/10.1016/j.aquabot.2018.08.002

Gerbersdorf, S.U., Westrich, B., Paterson, D.M., 2009. Microbial extracellular polymeric substances (eps) in fresh water sediments. Microbial Ecology 58, 334–349. https://doi.org/10.1007/s00248-009-9498-8

Guo, L., Dai, L., Zheng, J., Zhou, W., Peng, C., Li, D., Li, G., 2022. Environmental factors associated with the filamentous green algae *Cladophora* blooms: A mesocosm experiment in a shallow eutrophic lake. Journal of Environmental Management 313, 114977. https://doi.org/10.1016/j.jenvman.2022.114977

Hui, Y., Zhu, Z., Atkinson, J.F., Saharia, A.M., 2021. Impacts of phosphorus loading temporal pattern on benthic algae growth in Lake Ontario. Journal of Hydrology 598, 126449. https://doi.org/10.1016/j.jhydrol.2021.126449

Kawaguchi, T., Decho, A.W., 2002. A laboratory investigation of cyanobacterial extracellular polymeric secretions (eps) in influencing caco3 polymorphism. Journal of Crystal Growth 240, 230–235. https://doi.org/10.1016/s0022-0248(02)00918-1

Kirk, J.T.O., 1975. A theoretical analysis of the contribution of algal cells to the attenuation of light within natural waters i. General treatment of suspensions of pigmented cells. New Phytologist 75, 11–20. https://doi.org/10.1111/j.1469-8137.1975.tb01366.x

Li, L., Sun, H., Ren, C., Zhao, Z., Song, Y., Wang, M., Chen, S., Zhou, G., 2025. Synchronous removal of heavy metals and ammonia-nitrogen by magnesium ammonium phosphate (map)-enhanced microbial induced calcite precipitation (micp). Journal of Hazardous Materials 498, 139994. https://doi.org/10.1016/j.jhazmat.2025.139994

Li, W.-W., Zhang, H.-L., Sheng, G.-P., Yu, H.-Q., 2015. Roles of extracellular polymeric substances in enhanced biological phosphorus removal process. Water Research 86, 85–95. https://doi.org/10.1016/j.watres.2015.06.034

Li, Y., Jin, B., Wang, K., Song, L., Ren, L., Hou, Y., Gao, X., Zhan, X., Zhang, Q., 2022. Coordinatively-

intertwined dual anionic polysaccharides as binder with 3d network conducive for stable sei formation in advanced silicon-based anodes. Chemical Engineering Journal 429, 132235. https://doi.org/10.1016/j.cej.2021.132235

Liegertová, M., Malý, J., 2023. Gastropod mucus: Interdisciplinary perspectives on biological activities, applications, and strategic priorities. ACS Biomaterials Science & Engineering 9, 5567–5579. https://doi.org/10.1021/acsbiomaterials.3c01096

Lu, H., Wan, J., Li, J., Shao, H., Wu, Y., 2016. Periphytic biofilm: A buffer for phosphorus precipitation and release between sediments and water. Chemosphere 144, 2058–2064. https://doi.org/10.1016/j.chemosphere.2015.10.129

McCusker, M., Dove, A., Depew, D., Howell, E.T., 2023. Factors affecting *Cladophora* growth in the eastern basin of Lake Erie: Analysis of a monitoring dataset (2012–2019). Journal of Great Lakes Research 49, 790–808. https://doi.org/10.1016/j.jglr.2023.05.004

Murugavel, R., Choudhury, A., Walawalkar, M.G., Pothiraja, R., Rao, C.N.R., 2008. Metal complexes of organophosphate esters and open-framework metal phosphates: Synthesis, structure, transformations, and applications. Chemical Reviews 108, 3549–3655. https://doi.org/10.1021/cr000119q

Neu, T.R., Lawrence, J.R., 2006. Development and structure of microbial biofilms in river water studied by confocal laser scanning microscopy. FEMS Microbiology Ecology 24, 11–25. https://doi.org/10.1111/j.1574-6941.1997.tb00419.x

Oikawa, K., Goto-Yamada, S., Hayashi, Y., Takahashi, D., Kimori, Y., Shibata, M., Yoshimoto, K., Takemiya, A., Kondo, M., Hikino, K., Kato, A., Shimoda, K., Ueda, H., Uemura, M., Numata, K., Ohsumi, Y., Hara-Nishimura, I., Mano, S., Yamada, K., Nishimura, M., 2022. Pexophagy suppresses ros-induced damage in leaf cells under high-intensity light. Nature Communications 13. https://doi.org/10.1038/s41467-022-35138-z

Park, J.B.K., Montemezzani, V., Picken, C., Rendle, D., Sutherland, D.L., Hariz, H., Craggs, R.J., 2025. Optimizing algal harvest interval to enhance the performance of filamentous algal nutrient scrubbers (fans) treating agricultural drainage. Journal of Environmental Management 393, 126868. https://doi.org/10.1016/j.jenvman.2025.126868

Paul, E., Ochoa, J.C., Pechaud, Y., Liu, Y., Liné, A., 2012. Effect of shear stress and growth conditions on detachment and physical properties of biofilms. Water Research 46, 5499–5508. https://doi.org/10.1016/j.watres.2012.07.029

Penn, C.J., Bryant, R.B., Kleinman, P.J.A., Allen, A.L., 2007. Removing dissolved phosphorus from drainage ditch water with phosphorus sorbing materials. Journal of Soil and Water Conservation 62, 269–276. https://doi.org/10.1080/00224561.2007.12435961

Prazukin, A., Shadrin, N., Balycheva, D., Firsov, Y., Lee, R., Anufriieva, E., 2020. *Cladophora* spp. (Chlorophyta) modulate environment and create a habitat for microalgae in hypersaline waters. European Journal of Phycology 56, 231–243. https://doi.org/10.1080/09670262.2020.1814423

Prazukin, A., Shadrin, N., Latushkin, A., Anufriieva, E., 2025. Mats of green filamentous alga *Cladophora* in the hypersaline bay sivash: Distribution, structure, environment-forming role and resource potential. Regional Studies in Marine Science 82, 104031. https://doi.org/10.1016/j.rsma.2025.104031

Reiss, R.S., Lemmin, U., Barry, D.A., 2023. What role does stratification play during winter in wind-induced exchange between the multi-depth basins of a large lake (Lake Geneva)? Journal of Great Lakes Research 49, 406–421. https://doi.org/10.1016/j.jglr.2023.02.005

Schubert, N., Tuya, F., Peña, V., Horta, P.A., Salazar, V.W., Neves, P., Ribeiro, C., Otero-Ferrer, F., Espino, F., Schoenrock, K., Ragazzola, F., Olivé, I., Giaccone, T., Nannini, M., Mangano, M.C., Sará, G., Mancuso, F.P., Tantillo, M.F., Bosch-Belmar, M., Martin, S., Le Gall, L., Santos, R., Silva, J., 2024. "Pink power"—the importance of coralline algal beds in the oceanic carbon cycle. Nature Communications 15. https://doi.org/10.1038/s41467-024-52697-5

Serrano-Ruiz, J.C., Luque, R., Sepúlveda-Escribano, A., 2011. Transformations of biomass-derived platform molecules: From high added-value chemicals to fuels via aqueous-phase processing. Chemical Society Reviews 40, 5266. https://doi.org/10.1039/c1cs15131b

Shekhar, M., Shriwastav, A., Bose, P., Hameed, S., 2017. Microfiltration of algae: Impact of algal species, backwashing mode and duration of filtration cycle. Algal Research 23, 104–112. https://doi.org/10.1016/j.algal.2017.01.013

Song, C., Cao, X., Zhou, Y., Shadrin, N.V., 2017. Filamentous green algae, extracellular alkaline phosphatases and some features of the phosphorus cycle in ponds. Marine Biological Journal 2, 66–78. https://doi.org/10.21072/mbj.2017.02.1.07

Srisai, P., Suriyaprom, S., Panya, A., Pekkoh, J., Tragoolpua, Y., 2024. Inhibitory effects of algal polysaccharide extract from *Cladophora* spp. Against herpes simplex virus infection. Scientific Reports 14. https://doi.org/10.1038/s41598-024-60941-7

Staudt, C., Horn, H., Hempel, D.C., Neu, T.R., 2004. Volumetric measurements of bacterial cells and extracellular polymeric substance glycoconjugates in biofilms. Biotechnology and Bioengineering 88, 585–592. https://doi.org/10.1002/bit.20241

Stevenson, R.J., Stoermer, E.F., 1982. Luxury consumption of phosphorus by benthic algae. BioScience 32, 682–683. https://doi.org/10.2307/1308821

Surayot, U., Hun Lee, J., Kanongnuch, C., Peerapornpisal, Y., Park, W., You, S., 2016. Structural characterization of sulfated arabinans extracted from*Cladophora glomerata*kützing and their macrophage activation. Bioscience, Biotechnology, and Biochemistry 80, 972–982. https://doi.org/10.1080/09168451.2015.1132149

Wang, C., Liu, W., Chen, R., Liu, J., Yu, J., Liu, Q., Zhu, J., Sun, G., Li, Y., Wang, J., 2026. Polarity-driven marine antifouling coating with dynamic surface: Elucidating mechanism for disrupting mussel adhesion. ACS Applied Materials & Interfaces 18, 17014–17027. https://doi.org/10.1021/acsami.6c00682

Wang, Y., Wang, K., Bing, X., Tan, Y., Zhou, Q., Jiang, J., Zhu, Y., 2024. Influencing factors for the growth of *Cladophora* and its cell damage and destruction mechanism: Implication for prevention and treatment. Water 16, 1890. https://doi.org/10.3390/w16131890

Wu, Z., Yuan, X., Xiong, X., Ao, H., Wu, C., Liu, G., Zhu, H., 2024. *Cladophora* as ecological engineer: A new test from the largest lake of qinghai-tibet plateau with filamentous algal blooms. Water Biology and Security 3, 100210. https://doi.org/10.1016/j.watbs.2023.100210

Xie, R., Chang, M., Gao, Y., Chen, Y., 2025. Submerged macrophyte restoration drives microbial community reassembly and functional adaptation for synergistic water quality improvement. Total

Environment Microbiology 1, 100048. https://doi.org/10.1016/j.temicr.2025.100048

Xu, Y., Ou, Q., Zhou, X., He, Q., Wu, Z., Huang, R., Song, J., Ma, J., Huangfu, X., 2020. Impacts of carrier properties, environmental conditions and extracellular polymeric substances on biofilm formation of sieved fine particles from activated sludge. Science of The Total Environment 731, 139196. https://doi.org/10.1016/j.scitotenv.2020.139196

Yang, Y., Li, W., Li, Y., Xu, N., 2024. Effects of ocean acidification and nitrogen limitation on the growth and photophysiological performances of marine macroalgae gracilariopsis lemaneiformis. Frontiers in Marine Science 11. https://doi.org/10.3389/fmars.2024.1453569

Yunev, O.A., Carstensen, J., Moncheva, S., Khaliulin, A., Ærtebjerg, G., Nixon, S., 2007. Nutrient and phytoplankton trends on the western black sea shelf in response to cultural eutrophication and climate changes. Estuarine, Coastal and Shelf Science 74, 63–76. https://doi.org/10.1016/j.ecss.2007.03.030

Zhang, X., Devanadera, Ma.C.E., Roddick, F.A., Fan, L., Dalida, M.L.P., 2016. Impact of algal organic matter released from *Microcystis aeruginosa* and *Chlorella* sp. On the fouling of a ceramic microfiltration membrane. Water Research 103, 391–400. https://doi.org/10.1016/j.watres.2016.07.061

Zribi, I., Ellouzi, H., Mnasri, I., Abdelkader, N., Ben Hmida, A., Dorai, S., Debez, A., Charfi-Cheikhrouha, F., Zakhama-Sraieb, R., 2023. Effect of shading imposed by the algae *Chaeotomorpha linum* loads on structure, morphology and physiology of the seagrass cymodocea nodosa. Marine Environmental Research 188, 106001. https://doi.org/10.1016/j.marenvres.2023.106001

Zulkifly, S.B., Graham, J.M., Young, E.B., Mayer, R.J., Piotrowski, M.J., Smith, I., Graham, L.E., 2013. The genus *Cladophora K*ützing (ulvophyceae) as a globally distributed ecological engineer. Journal of Phycology 49, 1–17. https://doi.org/10.1111/jpy.12025